Chemical Engineering Journal 512 (2025) 162632

Contents lists available at ScienceDirect

Chemical Engineering Journal

journal homepage: www.elsevier.com/locate/cej

Enhanced trace gadolinium(III) extraction via tailored chemisorption on defect-engineered molybdenum disulfide electrodes

Weiquan Zhan [a,b,*], Yuan Yuan [c], Qizheng Weng [a], Yanan Pan [d], Shaoxian Song [f,*], José Luis Arauz-Lara [b], Feifei Jia [a,e,*], Wencai Zhang [d]

[a] Key Laboratory of Green Utilization of Critical Non-metallic Mineral Resources of Ministry of Education, Wuhan University of Technology, Wuhan 430070 Hubei, China
[b] Instituto de Física, Universidad Autónoma de San Luis Potosí, Av. Manuel Nava 6, Zona Universitaria, San Luis Potosí 78290, Mexico
[c] Doctorado Institucional de Ingeniería y Ciencia de Materiales, Universidad Autónoma de San Luis Potosí, Av. Sierra Leona 530, San Luis Potosí 78210, Mexico
[d] Department of Mining and Minerals Engineering, Virginia Polytechnic Institute and State University, Blacksburg, VA 24061, United States
[e] School of Resources and Environmental Engineering, Wuhan University of Technology, Wenzhi Street 34, Wuhan 430070 Hubei, China
[f] Instituto de Metalurgia, Universidad Autónoma de San Luis Potosí, Av. Sierra Leona 550, San Luis Potosí 78210, Mexico

ARTICLE INFO

Keywords:
Trace gadolinium(III)
Separation and recovery
Rich defects
MoS_2
Chemisorption modulation

ABSTRACT

Separation and recovery of trace gadolinium(III) from rare earth elements (REEs) with similar properties is increasingly crucial for renewable energy resources and sustainable development. This study proposed a method to regulate the chemisorption activity of gadolinium(III) using defects-rich molybdenum disulfide (DR-MoS_2) electrodes, enabling the separation and recovery of gadolinium(III) from aqueous solutions. Lanthanum(III), gadolinium(III), and yttrium(III), representing light, medium, and heavy REEs respectively, were selected to investigate their adsorption behaviors of on MoS_2 and DR-MoS_2 electrodes at low concentrations. Experiments and simulation results verified distinct adsorption behaviors of REEs on MoS_2, influenced by their out-shell electron binding capabilities. Interestingly, gadolinium(III) exhibited a unique interaction where its f orbitals strongly interacted with p orbitals of unsaturated sulfur atoms, unlike the other REEs, facilitating effective separation and recovery of gadolinium(III). Furthermore, increased binding affinity enhanced the electric double layer capacity (EDLC) and reduced electrons immigration resistance. Consequently, DR-MoS_2 electrodes achieved 100% recovery of trace gadolinium(III) recovery with high separation efficiency. Hopefully, strongest lanthanum(III) interaction with unsaturated Mo atoms was expected to realize lanthanum(III) separation and recovery. This study presented a promising approach to selectively recover target REEs from similar elements through modulating the chemisorption.

1. Introduction

Gadolinium (Gd) [1–3] is one of the rare earth elements (REEs) found within the lanthanide series, naturally occurring in the trivalent state. It presents unique properties of magnetic moment [4], attraction to thermal neutrons, thus being widely applied in neutron absorbers [5–7], magnetic resonance imaging [8–10], magnetic storage [11,12], and other vital fields [13]. Because of its trace amount in applications, Gd bypasses waste water treatment plants and be released into aquatic environments [14–16], while the toxicity characteristic brings threat to human [17]. The appearance of Gd blocks transfer of calcium(II) inside the body since similar ionic radius [18]. Herein, the recovery of trace amounts of Gd from aquatic solutions is becoming increasingly necessary.

Conventional techniques employed for separation or recovery of REEs include ion extraction [19–21], ion-exchange [22–24], chemical precipitation [25–27], and sorption [28–30] methods. Most of these methods suffer from high costs, as well as high chemical and energy consumption [31–33]. Even though sorption possesses the advantages of economics and environmental friendliness, there is still a long way to achieve efficient separation and recovery of Gd. Therefore, it is timely to explore an approach to separate and recover Gd to support the global green development goals.

Electrosorption [34–36] is a sorption process that involves ions

* Corresponding authors at: Key Laboratory of Green Utilization of Critical Non-metallic Mineral Resources of Ministry of Education, Wuhan University of Technology, Wuhan 430070, Hubei, China (Weiquan Zhan and Feifei Jia).
E-mail addresses: zhan_weiquan@163.com (W. Zhan), ssx851215@whut.edu.cn (S. Song), feifeijia@whut.edu.cn (F. Jia).

https://doi.org/10.1016/j.cej.2025.162632
Received 3 February 2025; Received in revised form 5 April 2025; Accepted 13 April 2025
Available online 16 April 2025

migrating in an electrolyte, interacting with the adsorbate, and being stored in electric double layer (EDL) under the influence of external electricity. Generated electric field is prone to facilitate the ions in aqueous solutions to immigrate to oppositely charged electrode, and being beneficial for targeted ions to overcome the electrostatic repulsion to interact with electrodes [37–39]. It has been demonstrated to be advantageous for the adsorption of metal ions such as lead(II) [40–42], copper(II) [43–45], nickel(II) [46–48], chromium [49–51], and others [52].

Considering that the interaction force between guest materials and target ions plays a crucial role in sorption, selecting suitable electrode materials that can strongly interact with Gd holds promise for achieving efficient separation and recovery. Molybdenum disulfide (MoS_2) with a sandwich structure of S-Mo-S is recognized as a potential electrode for REEs recovery through chemisorption and electrosorption coupling (CEC) process [53]. However, achieving selective adsorption is challenging due to the similar properties of REEs.

In view of the largest number of unpaired electrons in Gd among REEs, the configuration extra-nuclear electrons of Gd differs from that of others. According to valence bond theory, unsaturated S atoms have more lone pairs of electrons, which is favorable to bind with Gd. It is reported that MoS_2 with unsaturated S atoms show the great potential application merits in heavy metals. For instance, in our previous study, we engineered sulfur defects in MoS_2 primarily to enhance Pb^{2+} adsorption, where sulfur vacancies acted as dominant active sites for strong chemisorption of heavy metals [54]. Therefore, significant efforts are required to comprehend the separation and recovery of trace Gd from aqueous solutions using defects-rich MoS_2 electrodes.

Here, we propose the use of defects-rich MoS_2 (DR-MoS_2) electrodes achieved by controlling the ratio of S and Mo sources for the separation and recovery of Gd(III). Titanium plates were selected as substrates due to their excellent corrosion resistance, high electrical conductivity, and good mechanical stability [55]. These properties make titanium plates suitable for serving as stable conductive substrates for electrode preparation, especially under harsh electrochemical conditions. DR-MoS_2 was coated on the surface of titanium plate to induce Gd immigration and overcome electrostatic repulsion between material interface and target ions. La(III), Gd(III), and Y(III) as respectively represented light, medium, and heavy REEs were chosen for studying the sorption behaviors of REEs on DR-MoS_2 electrodes. The experimental results on Gd separation and recovery revealed efficient recovery performances via DR-MoS_2 electrodes, which was consistent with our prediction. Gd(III) recovery though adjusting the interaction between materials and target on a CEC process in the work helps to guide a thought for targeted trace REEs recovery.

2. Reagents and methods

2.1. Reagents

Lanthanum nitrate hexahydrate ($LaN_3O_9{\cdot}6H_2O$, 99.9 %), gadolinium nitrate hexahydrate ($GdN_3O_9{\cdot}6H_2O$, 99.9 %), and yttrium nitrate hexahydrate ($YN_3O_9{\cdot}6H_2O$, 99.9 %) were bought from Aladdin Co., China. Conductive carbon black was originated from the Cabot Corporation. Ammonium molybdate tetrahydrate ($(NH_4)_6Mo_7O_{24}{\cdot}4H_2O$), thiourea ($CN_2H_4S$), hydrochloric acid (HCl), nitric acid (HNO_3), sodium hydroxide (NaOH), Polytetrafluoroethylene ($(C_2F_4)_n$), ammonium chloride (NH_4Cl), and sodium sulfate (Na_2SO_4) were purchased from Sinopharm Chemical Reagent Co., Ltd., China. Deionized water (18.2 MΩ cm) produced by Millipore Super Q system was throughout the whole experiment.

2.2. Samples preparation

Synthesis of DR-MoS_2 was done via adjusting the ratio of Mo and S sources (1:2, 1:3, 1:4, and 1:5) in the hydrothermal route. Mo ($(NH_4)_6Mo_7O_{24}{\cdot}4H_2O$) and S ($CN_2H_4S$) sources were dissolved in 72 mL distilled water by stirring. Later, the solution was transferred into a 100 mL Teflon-lined stainless-steel autoclave at 220 °C for 18 h. After cooling down to room temperature, the obtained products were washed with pure water and ethanol. Lastly, the black products were dried at −60 °C in vacuum environment for 12 h. The obtained samples were named as MoS_2, DR1-MoS_2, DR2-MoS_2, and DR3-MoS_2 according to various ratio of Mo and S sources.

2.3. Electrodes fabrication

DR-MoS_2 was coated on the surface of titanium plate to fabricate electrode. The mixture including 80 mg DR-MoS_2, 10 mg conductive carbon black, and 0.8 mL polyvinylidene fluoride was grinded in sapphire mortar. After, the samples were coated on surface of titanium plate and heated at 60 °C for 3 h to remove excess organic reagents. In the end, the prepared electrodes were immerged in pure water for 12 h, then being dried for 6 h at 60 °C.

2.4. REEs recovery

La(III), Gd(III), and Y(III) were respectively chosen as light, medium, and heavy REEs to study the REEs recovery behaviors on DR-MoS_2 electrodes. The recovery experiments were carried out in a self-made cell with an external applied voltage of 0.8 V. 200 mL REEs solution with pH of 5 was recycled with rate of 45 rpm by a peristaltic pump. Reacting after a certain time, the solution extracted from the cell was detected using UV–Vis spectrophotometer (Aquamate 8000, Lambda 750S). Firstly, a certain amount of REEs was dissolved in a 100 mL volumetric flask to obtain a 2000 mg/L standard solution. Subsequently, various concentrations of REEs solutions were prepared by mixing with 2 mL arsenazo III (0.5 g/L) in a 25 mL colorimetric tube. The method offers simplicity and rapid detection with acceptable sensitivity for individual REEs solution. Related recovery performances were assessed by adsorption capacity (Q) and recovery (R) as following equations:

$$Q = \frac{C_0 V_0 - C_t V_t}{Am} \tag{1}$$

$$R = \frac{C_0 - C_t}{C_0} \tag{2}$$

where C_0 and C_t respectively mean REEs concentration at the beginning and t moments in the recovery process, mg/L, V_0 and V_t respectively represent the volumes of reaction solution at the beginning and t moments, L, A is surface area for coated samples on titanium plate, dm^2, and m stands for the mass of samples in the coating mixture, mg.

2.5. Gd(III) separation

According to the various sorption behaviors of REEs on DR-MoS_2 electrodes, trace Gd(III) separation from the other two kind of REEs (La (III), and Y(III)) was performed. Specifically, the mixture including La (III), Gd(III), and Y(III) at 1 mg/L each at pH of 5 was applied on studying Gd(III) separation recovery by DR-MoS_2 electrodes with external applied voltage of 0.8 V. The concentration of all REEs was analyzed by inductively coupled plasma-optical emission spectrometry (ICP-OES, Prodigy 7, America). ICP-OES was selected for its high sensitivity, broad dynamic range, and capability to simultaneously detect multiple elements with good accuracy and precision. Its detection limits (approximately 0.5–1 μg/L for Gd(III), Y(III), and La(III)) are sufficient for evaluating the adsorption and separation performance of the DR-MoS_2 electrodes. Separation coefficient of Gd(III) ($S_{Gd(III)/REE}$) was calculated as below equations:

$$D_{REE} = \left(\frac{C_0 - C_t}{C_t}\right) \times \left(\frac{V_t}{V_{srp}}\right) \tag{3}$$

$$S_{Gd(III)/REE} = \frac{D_{Gd(III)}}{D_{REE}} \quad (4)$$

where D is the distribution ration, V_{srp} represents the volume in desorption aqueous solutions, mL.

2.6. Gd(III) desorption

To reveal the adsorbed amount on DR-MoS_2 electrodes, Gd(III) desorption was performed in 1 M NH_4Cl or 1 M HCl solution with 200 mL volume for 2 h. The desorption efficiency was calculated as:

$$D_e = \frac{C_d}{C_0} \quad (5)$$

where C_d is the concentration of Gd(III) in the solution in HCl or NH_4Cl during the desorption process, mg/L.

2.7. Interaction simulations

With the aim of understanding selective Gd(III) sorption from mixed REEs solutions, simulations for interaction of La(III), Gd(III), and Y(III) on the interface of DR-MoS_2 through density functional theory were calculated (DMol3 program). The Generalized Gradient Approximation (GGA) together with Perdew-Bruke-Ernzerhof (PBE) was used for describing exchange and correlation between electrons. The electron relaxation with 10^{-5} eV and energy cutoff with 320 eV were set for auxiliary plane waves. Applying vacuum with 20 Å length was to avoid the interaction with neighboring images. Adsorption energy of REEs (E_{ads}) on DR-MoS_2 was calculated as:

$$E_{ads} = E_{REE+DR-MoS2} - E_{DR-MoS2} - E_{REE} \quad (6)$$

where $E_{REE+DR-MoS2}$ represents the total energy after interaction, $E_{DR-MoS2}$ is the energy of DR-MoS_2, and E_{REE} is the energy of REE.

2.8. AFM measurement

The adsorption process of Gd(III) on surface of MoS_2 with edge defects was observed by the atomic force microscope (AFM, Bruker Multimode 8 system, Billerica). MoS_2 sample was directly cut into a bulk with fresh surface and used owing to its natural property of sandwich-like structure. Gd(III) solution with 10 mg/L was dropped on the freshly exposed surface of MoS_2 with edge defects. After being reacted at a certain time, the residual solution was removed by filter paper. AFM was performed on observing the morphology after drying.

2.9. Electrochemical test

Electrochemical characteristics containing cyclic voltammetry (CV) and electrochemical impedance spectroscopy (EIS) were detected with a conventional three-electrode cell in the REEs solution through electrochemical workstation (VersaSTAT-450, RAR, America). Three electrodes contained working electrode with samples, counter electrode with platinum, and reference electrode with a standard calomel. Preparation of working electrode (samples, conductive carbon black, and polytetrafluoroethylene) was via the same procedure applied in recovery experiment.

2.10. Material characterization

Crystal structure was obtained through X-ray diffraction (XRD) with Cu-Kα radiation (D8 Advance, Bruker AXS, Germany). Morphology was characterized through scanning electron microscopy (SEM, Phenom ProX G6, Netherlands) and transmission electron microscopy (TEM, JEM-F200, Japan). Elemental state information was gained through X-ray photoelectron spectroscopy (XPS, Thermo Scientific K-Alpha, America). Raman (INVIA, Renishaw, England) was conducted on testing atomic bond structure.

3. Results and discussion

3.1. Phase and morphology

DR-MoS_2 was produced by one-pot thermal synthesis using our previously reported method [54]. Samples were prepared by adjusting the ratio of Mo and S sources, and there were more unsaturated S atoms in the structure of MoS_2 when higher of S resource concentration than Mo resource concentration in the reaction atmosphere. Fig. 1a showed the structure of samples provided by XRD patterns. Peaks of characteristic diffraction at 14°, 33°, 39°, and 58° were respectively indexed to (002), (100), (103), and (110) plane of 2H-MoS_2 (JCPDS 37–1492) [56]. Shape of the peaks kept unchanged, while being little weakened in atom interferometer direction, expressing that the microstructure was well preserved. To gain deeper insights about defects in the structure of MoS_2, we performed Raman spectra measurement (Fig. 1b) on the samples. As could be seen, the two peaks were attributed to binding layer between Mo and S atoms (E^1_{2g} mode) and out-of-plane vibration of S atoms (A_{1g} mode) [57]. Shift of peaks to lower wavenumbers suggested the occurrence of defects when more S sources in synthesis process were added. Further, peak intensity ratio of E^1_{2g} and A_{1g} declined as higher dosage of sources (Fig. 1c), demonstrating the existence of more exposure defects with unsaturated S atoms [58]. Additionally, ICP analysis (Fig. S1) provided quantitative evidence of defect modulation, showing that the molar ratio of S to Mo increased as the S source concentration was elevated. By precisely tuning the ratio of Mo and S sources, it is possible to effectively regulate defect concentration and optimize the MoS_2's functional properties.

To identify the morphology, TEM and HRTEM images of DR-MoS_2 were taken and shown in Fig. 1d, e. Nanosheets with ultrathin edges were uniformly distributed, and (002) and (101) crystal facets of MoS_2 were found through selected area electron diffraction (SAED) result. Slightly alterative interlayer distance compared to normal value (Fig. 1f) exhibited the presence of lattice distortion. As marked in origine circles and the height profile of fringe, the lamellar structures appeared broken due to the defects. EDS mapping (Fig. 1g) further displayed the homogeneous distribution of Mo and S elements across the samples, while a weak existence of O, resulting from MoS_2 distortion. These observations confirm that DR-MoS_2 was successfully synthesized by regulating the Mo and S sources rations.

3.2. REEs sorption behaviors and electrodes reusability

Given the interaction between REEs and DR-MoS_2, REEs sorption on MoS_2 and DR-MoS_2 electrodes via CEC process was investigated. Fig. 2a and 2b clearly indicated that the adsorption capacity and recovery of Gd (III) on MoS_2 and DR-MoS_2 were highest, and Y(III) took second place, which was related with the binding ability between REEs and electrodes. As introducing more defects into the structure of MoS_2, adsorption capacity and recovery of REEs were all enhanced, verifying that defective structure was beneficial for interaction with REEs. Interestingly, the recovery ability of Gd(III) was mostly obvious because the largest number of unpaired electrons in Gd(III) would strongly interact with unsaturated S atoms in MoS_2. DR-MoS_2 electrodes were applied to determine the adsorption kinetics of La(III), Gd(III), and Y(III). Upon applying a fixed external voltage, REEs adsorption capacity quickly increased and then tended to be stable by a gradual increased time, suggesting the gradual saturation of ions sorption on DR-MoS_2 electrodes. Additionally, it was apparent that the adsorption capacity of REEs followed the order of Gd(III)>Y(III)>La(III), which might be relevant to interaction between outer atomic orbital of REEs and DR-MoS_2.

The data was analyzed using the pseudo first and second order

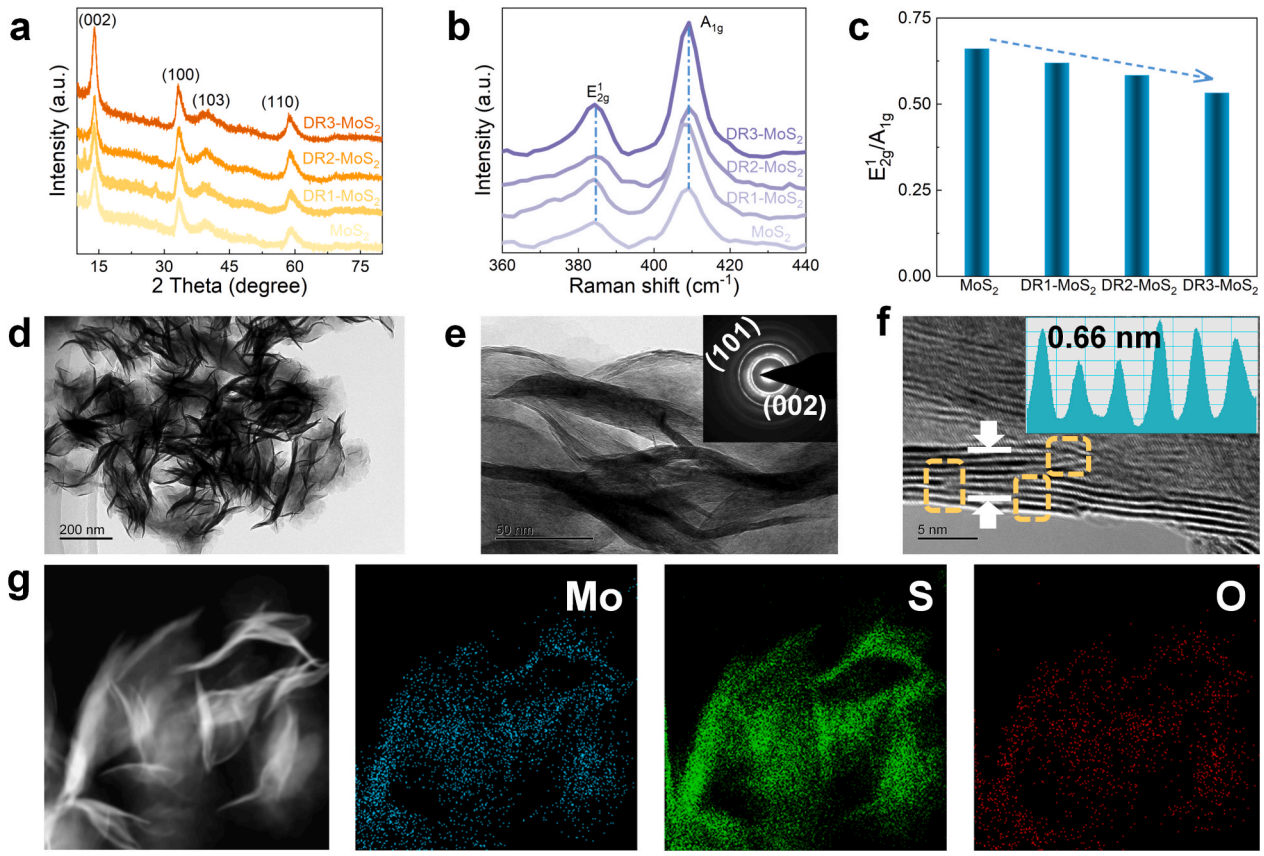

Fig. 1. Structure and morphology characterization of samples prepared with various concentrations of S and Mo sources in synthesis process. (a) XRD patterns, (b) Raman spectra, and (c) ratio of E^1_{2g} and A_{1g} intensity. (d) TEM, and (e, f) HRTEM images of DR-MoS_2, insert picture in e and f were SAED image and height profile of fringe, respectively. (g) TEM and corresponding EDS mapping of DR-MoS_2.

models as denoted respectively by following equations.

$$q_t = q_e \times [1 - \exp(-k_1 t)] \tag{7}$$

$$q_t = \frac{t}{\left(\frac{t}{q_e}\right) + \left(\frac{1}{k_2 q_e^2}\right)} \tag{8}$$

where q_e and q_t were adsorption capacity at equilibrium and t moment, respectively, min, k_1 and k_2 represented the rate constants for first and second order models, respectively, min^{-1}.

Data fitted well with the model, and the fitting parameters were obtained in Fig. 2c and Table S1. The proposed models aligned closely with the experimental data, providing a solid description of REEs adsorption, despite slight deviations in simulating adsorption for all REEs. Both models fitted the La(III) adsorption process well, while pseudo-second-order model dominated for Gd(III) and Y(III) adsorption. Specially it is noted that the adsorption capacity of REEs follows the order of Gd(III) > Y(III) > La(III), which might be related to the interaction ability of the outer atomic orbitals between REEs and DR-MoS_2. The maximum adsorption capacity of Gd(III) was found to be 299.32 mg/(g·dm^2) under the conditions of electrodes-distance of 3 mm and initial concentration of 10 mg/L. This highlights the significance of strong chemical interactions in Gd(III) recovery.

To further explore DR-MoS_2 electrode performance, adsorption capacity and recovery of La(III), Gd(III), and Y(III) at different initial concentrations were investigated (Fig. 2d-f). Results showed adsorption capacity increased with concentration, while recovery slightly dropped for La(III) and Y(III) due to the saturated active sites. Gd(III) recovery remained almost 100 % under the conditions of concentrations from 0.1 to 5 mg/L and electrodes-distance of 3 mm. Compared with previous studies on Gd(III) recovery (Table S2), our material and method show remarkable advantages. Fig. 2g-i presented SEM and EDS patterns after recovery, indicating REEs adsorption without altering DR-MoS_2's morphology. These differences suggest the potential to separate Gd(III) from La(III) and Y(III), which share similar properties.

To assess the cyclic stability of the DR-MoS_2 electrodes, we performed desorption of Gd(III) using HCl (Fig. S2) and NH_4Cl (Fig. S3) for 2 h. Both reagents effectively desorbed Gd(III), achieving complete desorption in the first cycle. However, the DR-MoS_2 electrodes treated with NH_4Cl exhibited better cyclic performance compared to that treated with HCl, possibly because HCl can deteriorate the active sites of DR-MoS_2. Nevertheless, repeated use of NH_4Cl for desorption may gradually compromise the electrode's adhesion and structural integrity, resulting in a decrease in Gd(III) recovery. The above results indicate that for further industrial application, it is necessary to improve the adhesion of the coated electrodes and enhance the stability of the electrode materials.

3.3. *Optimization experiments and Gd(III) separation*

Generally, operation parameters including electrodes-distance, solution pH, and applied voltage were researched on Gd(III) recovery performances. Appropriate electrodes-distance (Fig. 3a) operated in favor of recovery. Short electrodes-distance decelerated the flow of reaction solutions, while long electrodes-distance weakened the immigration of target ions in solutions. Adsorption capacity and recovery of Gd(III) as a function of pH medium was given in Fig. 3b. According to the figure, the adsorption was enhanced up to pH of 5, and then being declined as higher than 5. pH influenced metal ions adsorption either by causing the variation of adsorption sites or by altering the charged

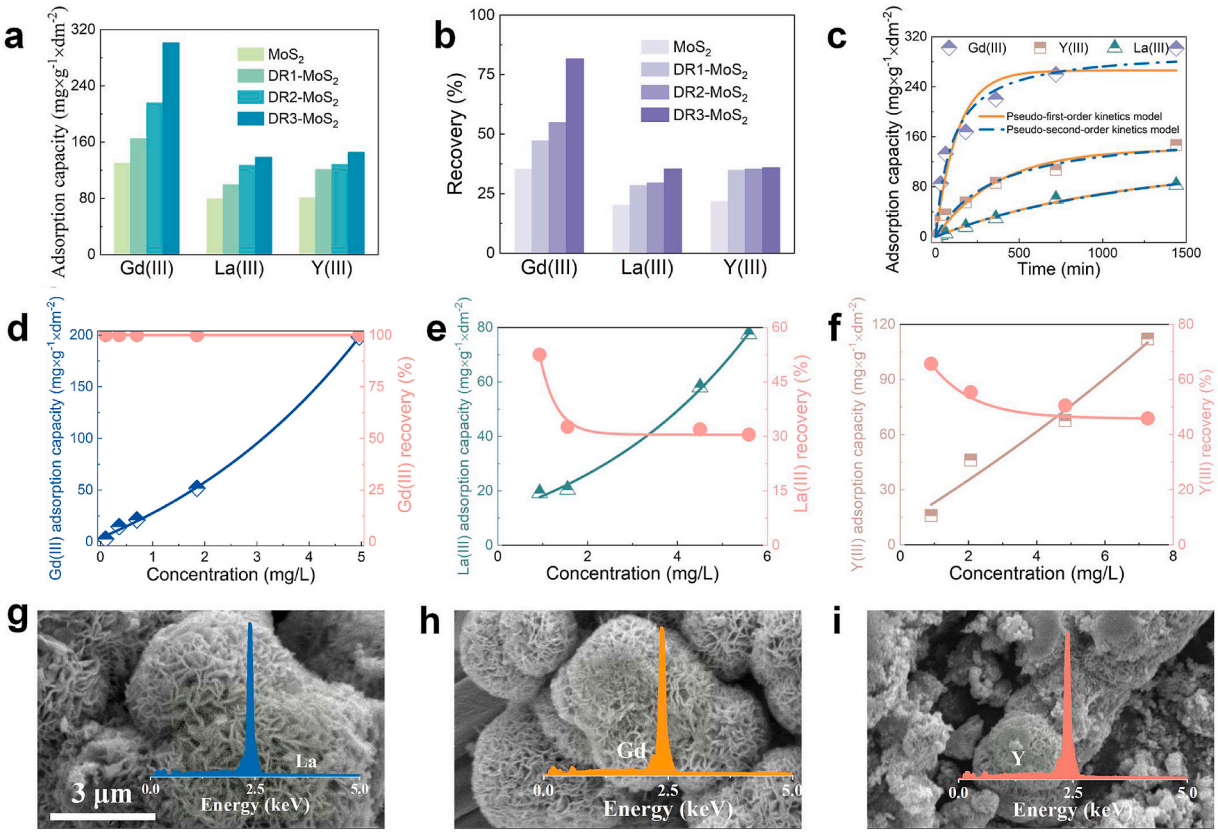

Fig. 2. (a) Adsorption capacity, and (b) corresponding recovery of La(III), Gd(III), and Y(III) on MoS_2 and DR-MoS_2 electrodes. (c) Adsorption kinetics of La(III), Gd (III), and Y(III) on DR-MoS_2 electrodes. (d) Gd(III), (e) La(III), and (f) Y(III) adsorption capacity and corresponding recovery at various initial concentrations on DR-MoS_2 electrodes. SEM and corresponding EDS pattern of DR-MoS_2 electrodes after (g) La(III), (h) Gd(III), and (i) Y(III) recovery.

species of ions. Upon the increasement of pH, deprotonation of DR-MoS_2 increased, thus to push up number of interacted sites. As for decreased adsorption under high pH value, the changeable species of Gd(III) with more hydration molecules would lessen the interaction with DR-MoS_2. Effects of applied voltage on the CEC process of Gd(III) recovery was investigated (Fig. 3c). It was noted that adsorption capacity and recovery were significantly improved at a certain mini charging voltage. External electric field caused by voltage facilitated the immigration of ions toward electrodes, thus enhancing the recovery performances. Besides, the charged electrodes were beneficial for the interaction of Gd (III). However, when the applied voltage was increased to 1.2 V, noticeable hydrogen evolution began to occur due to the water electrolysis process. This is because the applied voltage exceeded the water splitting threshold, resulting in the formation of hydrogen gas at the electrode surface. At 1.6 V, hydrogen evolution became even more pronounced, leading to a significant reduction in the recovery due to electrode surface coverage by gas bubbles and competition of active sites.

Evaluating Gd(III) separation performances from La(III) and Y(III) was necessary for the application of CEC method with DR-MoS_2 electrodes in REEs separation. The experiment was performed in a mixture solutions including La(III), Gd(III), and Y(III). Related separation coefficients of Gd(III) with two REEs were calculated and exhibited in Fig. 3d. Gd(III) separation coefficient from Y(III) (8.35) was higher than that from La(III) (7.48), demonstrating the competition of Gd(III) and Y (III) on reactive sites for chemisorption. Due to the higher charge density and stronger interaction affinity of Gd(III) with DR-MoS_2 electrodes, Gd (III) more effectively excludes Y(III) from adsorption sites, resulting in higher separation coefficient. Compared with previous studies on the separation coefficients of Gd(III) from La(III) and Y(III) reported in the literature (Table S3), our material and method demonstrate significant advantages. XPS analysis was conducted to obtain further information on the surficial interaction of REES and DR-MoS_2. The survey scan (Fig. 3e) revealed that DR-MoS_2 was composed of three elements, i.e., Mo, S, and O. After REEs recovery, there appeared three new peaks of La, Gd, and Y elements, demonstrating the adsorption of La(III), Gd(III), and Y(III) on DR-MoS_2 electrodes (also be verified in SEM-EDS results of DR-MoS_2 electrodes after REEs recovery as seen in Fig. 3f). From Fig. 3g, it was observed that the Mo 3*d* spectra were deconvoluted into four species peaks. Peaks at ~ 231.9 and 228.8 eV were attributed to ^{IV}Mo, which was assigned to Mo-S bonds in MoS_2 [59]. The doublet peaks at ~ 234.9 and 229.9 eV corresponded to the ^{VI}Mo for the distortion of MoS_2. The other peaks at ~ 232.9 and 230.8 eV indicated the existence of 1 T phase MoS_2, which would be induced by the generation of edges. Referring to the S 2*p* spectra (Fig. 3h), the characteristic peaks at ~ 162.8 and 161.6 eV were belonging to S^{2-} in MoS_2, while peak at ~ 163.4 eV originated from S_2^{2-} owing to introduction of defects in the structure [60,61]. In the spectra of O 1*s* (Fig. 3i), the divided peaks at ~ 531.6 and 533.2 eV were ascribed to adsorbed water and $MoS_{2-x}O_x$, respectively [62]. Compared with the peaks of Mo, S, and O elements in DR-MoS_2 before recovery, the peaks apparently shifted to higher binding energy, which confirmed the strong interaction of REEs with DR-MoS_2.

3.4. Competitive Gd(III) capture

The electrochemical performances of MoS_2 and DR-MoS_2 electrodes were tested by cyclic voltammetry (CV) and EIS in Gd(III) solution. Obviously, there were no redox peaks in CV plots (Fig. 4a), and all the curves displayed analogous rectangular patterns, which revealed happen of typical electric double layer capacitor form. The enclosed area was positively correlated with electric double layer capacity (EDLC). By introducing more defects into the structure of MoS_2, corresponding

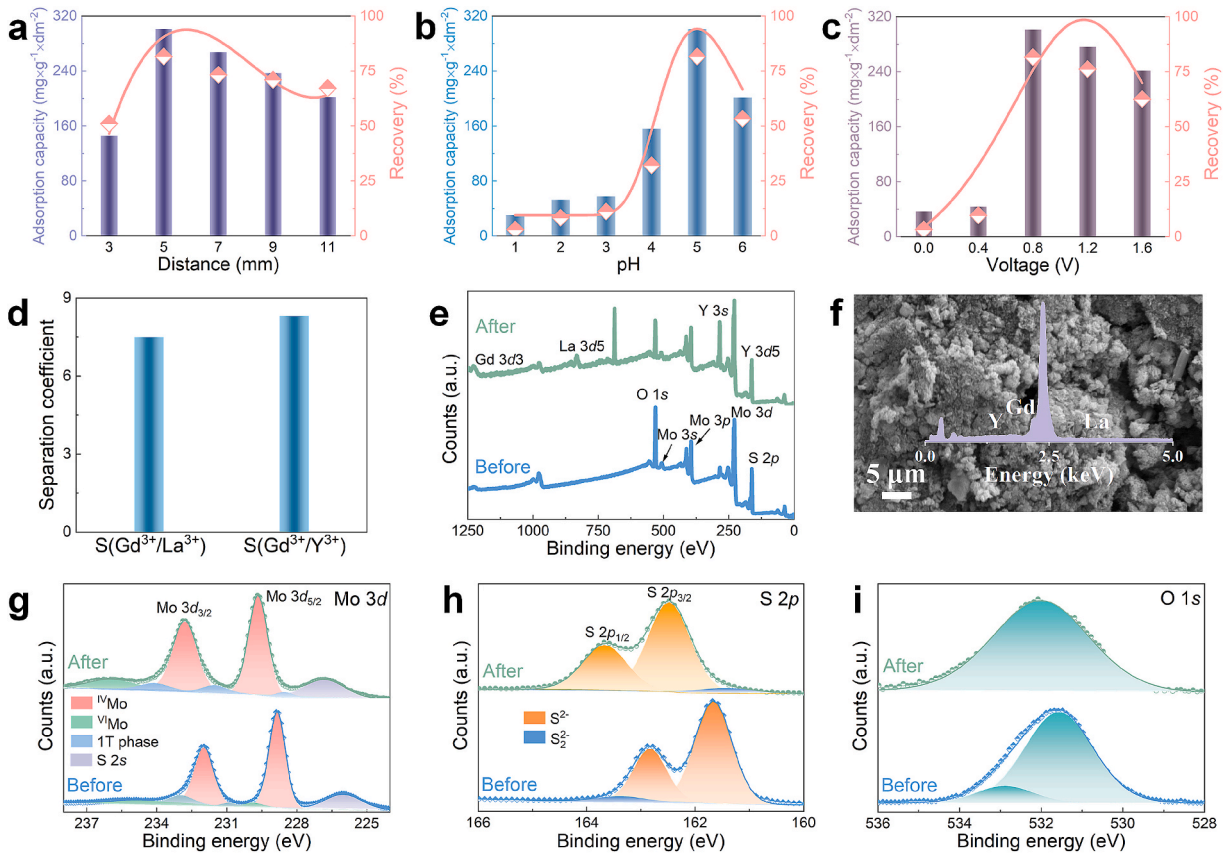

Fig. 3. Effect of operational parameters on Gd(III) recovery via DR-MoS_2 electrodes: (a) electrodes-distance, (b) solution pH, and (c) applied voltage. (d) Separation coefficient of Gd(III) in the mixture solution with La(III), Gd(III), and Y(III). XPS spectra: (e) survey spectra, (g) Mo 3*d*, (h) S 2*p*, and (i) O 1 *s* of DR-MoS_2 electrodes before and after recovery in REEs mixture solutions. (f) SEM and corresponding EDS pattern of DR-MoS_2 electrode after REEs recovery.

EDLC gradually increased, demonstrating that rich defects was in favor of Gd(III) adsorption. Compared with DR-MoS_2 electrode in La(III) and Y (III) solutions (Fig. S4), highest EDLC performance in Gd(III) solution suggested a strong ability in Gd(III) separation and recovery from other REEs using DR-MoS_2 electrode, which was consistent with the separation results (Fig. 3d). Moreover, EIS tests of MoS_2 and DR-MoS_2 electrodes were conducted to examine the resistance of ion immigration, as shown in Fig. 4b. Higher radius of semicircle represented greater ion immigration resistance. It was clear that DR-MoS_2 electrode possessed a lower ion immigration resistance in comparison with MoS_2, and more defects facilitated the immigration. As the defect concentration increases, the contact resistance decreases, enhancing the electronic conductivity of MoS_2. The improved contact resistance is attributed to the formation of defects with a lower Schottky barrier compared to pristine MoS_2. This is primarily because the defects provide additional active sites and create favorable pathways for electron migration, thereby promoting rapid charge transfer between the electrode surface and the electrolyte. What's more, strongest ion immigration ability of DR-MoS_2 electrode in Gd(III) solution, compared with EIS results of DR-MoS_2 electrode in La(III) and Y(III) solution (Fig. S5), strengthening Gd (III) recovery in REEs solutions. To verify Gd(III) adsorption on defects of MoS_2, AFM was applied to investigate MoS_2 with edge defects after being exposed to Gd(III) solution. The presence of defects in the AFM images was confirmed by measuring the thickness difference along the grey lines in Fig. 4c between two ends. As shown in Fig. S6, a thickness difference of approximately 100 pm was observed, indicating the presence of "edges" associated with defect sites. It was worth noticing that Gd(III) tended to interact the edge of DR-MoS_2. The adsorption layer thickness was around 143 pm, might be ascribed to the multilayer adsorption.

For the purpose of studying competitive Gd(III) adsorption on DR-MoS_2, DFT was performed to research the interaction of La(III), Gd(III), and Y(III) with MoS_2 and DR-MoS_2. Initially, possible structure of MoS_2 (Fig. S7a) and DR-MoS_2 with one S (Fig. S7b) (or Mo, Fig. S7c) atom loss as cycled in dotted line were optimized. Then, La(III), Gd(III), and Y(III) adsorption on the surface of three possible structure were calculated. After calculation, the balanced structures for adsorption from top and side views were provided in Fig. S8 and 4d-f. Closest distance of Y(III) rather than La(III) and Gd(III) to the surface of MoS_2, indicating strongest interaction of Y(III) with MoS_2. As for the surface of MoS_2-S, La(III) bound most tightly among the three REEs due to the attraction of unsaturated Mo atom. Interestingly, the interaction behaviors of REEs on the surface of MoS_2-Mo were different from the other two surfaces, and Gd(III) was most strongly adsorbed. Various REEs adsorption behaviors on MoS_2 and DR-MoS_2 were demonstrated via adsorption energy (Fig. 4g and Table S4). There were little differences in the adsorption of three REEs on MoS_2. Gd(III) and Y(III) interaction on the surface of MoS_2-Mo worked the best, while strong interaction of La(III) happened on the surface of MoS_2-S. From the data presented, it is evident that unsaturated S defects (MoS_2-Mo) exhibit significantly higher adsorption energies for Gd^{3+} compared to compared to Y^{3+} and La^{3+}, confirming the preferential adsorption of Gd^{3+} on DR-MoS_2. To reveal which binding atoms dominated the interaction, Mulliken atomic charge changes were performed to investigate La, Gd, Y, S and Mo atoms (Fig. 4h). As displayed, great force between REEs and MoS_2 (or DR-MoS_2) resulted from atomic charge changes in Mo and S atoms. The total lost charges in Mo and S atoms for three REEs were similar, but various REEs gained different distributed charges owing to the diverse interaction. In the sorption of MoS_2-Mo, Gd(III) exhibited the most efficient charge transfer capability during the interaction. Further, the binding

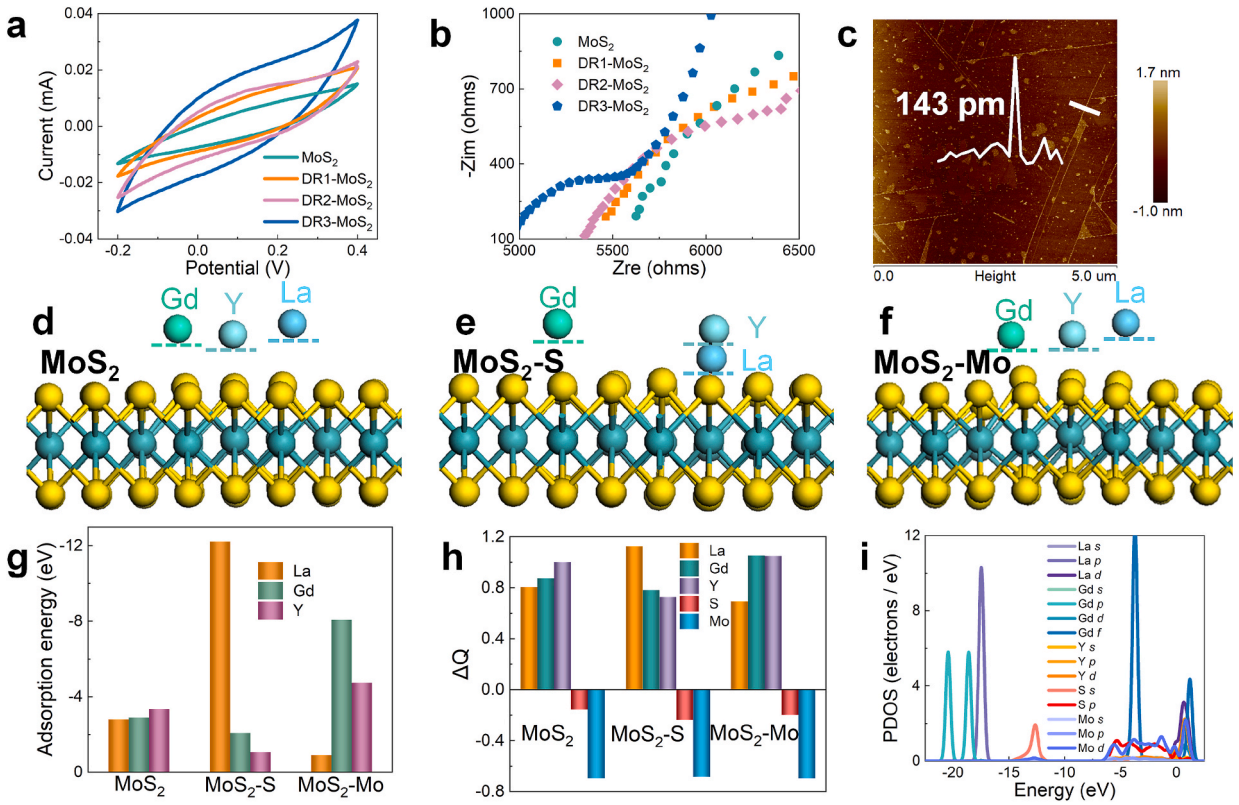

Fig. 4. (a) CV plots and (b) EIS results of MoS_2 and DR-MoS_2 electrodes in Gd(III) solutions. (c) AFM image of MoS_2 with edge defects after being exposed to Gd(III) solution for 2 h. Side configuration views of La(III), Gd(III), and Y(III) competition adsorption on the surface of (d) MoS_2, (e) MoS_2-S, and (f) MoS_2-Mo. (g) Adsorption energies of La(III), Gd(III), and Y(III) on MoS_2, MoS_2-S, and MoS_2-Mo. (h) Mulliken atomic charge changes of La(III), Gd(III), Y(III), S, and Mo in the system of REEs competition adsorption on MoS_2, MoS_2-S, and MoS_2-Mo. (i) PDOS of La(III), Gd(III), Y(III), S and Mo in the system of REEs competition adsorption on MoS_2-Mo.

orbitals between REEs and electrodes were investigated by partial density of states (PDOS). Each REE was tightly bound with S atoms, particularly with the *p* orbitals, on the electrode surface (Fig. 4i, S9 and S10). Compared with La(III) and Y(III), *f* orbitals in Gd(III) greatly participated in the interaction with unsaturated S atoms on MoS_2-Mo. The participation of the f orbitals of Gd^{3+} in bonding with unsaturated S atoms provides a significantly stronger interaction compared to La^{3+} and Y^{3+}, where such orbital overlap is less effective. Additionally, the electronic structure of Gd^{3+}, with half-filled 4f orbitals, enhances the stability of its adsorption with unsaturated S atoms on MoS_2 through stronger hybridization with the electrode surface. These findings provide a mechanistic understanding of why Gd^{3+} exhibits superior adsorption behavior over La^{3+} and Y^{3+}, beyond simple electron configuration differences. As well, the interaction of *d* orbitals in La(III) and *d* orbitals in unsaturated Mo atoms facilitated La(III) adsorption on MoS_2-S. Therefore, disparate extranuclear atomic orbital interaction led to significantly different chemical interaction.

4. Conclusion

Separation and recovery of trace Gd(III) from other similar REEs in aqueous solutions via regulating the chemisorption activity of electrodes was presented. Gd(III) recovery remained nearly 100 % under the conditions of a concentration from 0.1 to 5 mg/L, an applied voltage of 0.8 V, and electrodes-distance of 3 mm. The maximum adsorption capacity achieved was 299.32 mg/(g·dm^2) under the conditions of an initial concentration of 10 mg/L. In the competitive adsorption experiments, Gd(III) could be highly separated from La(III) and Y(III) because of special interaction *f* orbitals of Gd(III) with *p* orbitals of unsaturated S atoms in DR-MoS_2. In the meantime, super sorption ability enhanced EDLC and weakened charge transfer resistance of electrode in the solution to strengthen the electrochemical properties of electrodes. Remarkable, strong binding interaction between La(III) and unsaturated Mo atoms had the possibility to realize La(III) separation and recovery via MoS_2 with unsaturated Mo atoms defects. Thus, this work might benefit separation and recovery of target trace REEs from aqueous solutions by modulating chemisorption.

CRediT authorship contribution statement

Weiquan Zhan: Writing – review & editing, Writing – original draft, Investigation, Formal analysis. **Yuan Yuan:** Supervision, Formal analysis, Data curation. **Qizheng Weng:** Methodology, Investigation, Data curation. **Yanan Pan:** Validation, Supervision. **Shaoxian Song:** Visualization, Investigation. **José Luis Arauz-Lara:** Formal analysis. **Feifei Jia:** Writing – review & editing, Funding acquisition. **Wencai Zhang:** Resources, Conceptualization.

Declaration of competing interest

The authors declare that they have no known competing financial interests or personal relationships that could have appeared to influence the work reported in this paper.

Acknowledgements

The work is financially supported by the Natural Science Foundation of Hubei Province (ZRJQ2022000195) and National Natural Science Foundation of China (Grant No. 52274268 and No. 52422406). Weiquan Zhan gratefully acknowledges the Consejo Nacional de Humanidades Ciencias y Tecnologías (CONAHCYT) of Mexico for offering him the scholarship under the grant No. 813934 during his Ph.D. study.

Appendix A. Supplementary data

Supplementary data to this article can be found online at https://doi.org/10.1016/j.cej.2025.162632.

Data availability

Data will be made available on request.

References

[1] G. Wang, J. Xu, L. Ran, R. Zhu, B. Ling, X. Liang, S. Kang, Y. Wang, J. Wei, L. Ma, Y. Zhuang, J. Zhu, H. He, A green and efficient technology to recover rare earth elements from weathering crusts, Nat. Sustainability 6 (2022) 81–92, https://doi.org/10.1038/s41893-022-00989-3.

[2] L. Moriggi, C. Cannizzo, E. Dumas, C.R. Mayer, A. Ulianov, L. Helm, Gold nanoparticles functionalized with gadolinium chelates as high-relaxivity MRI contrast agents, J. Am. Chem. Soc. 131 (2009) 10828–10829, https://doi.org/10.1021/JA904094T.

[3] P. Miéville, S. Jannin, L. Helm, G. Bodenhausen, Kinetics of yttrium-Ligand complexation monitored using hyperpolarized 89Y as a model for gadolinium in contrast agents, J. Am. Chem. Soc. 132 (2010) 5006–5007, https://doi.org/10.1021/JA1013954.

[4] G.J. Stasiuk, S. Tamang, D. Imbert, C. Poillot, M. Giardiello, C. Tisseyre, E. L. Barbier, P.H. Fries, M. De Waard, P. Reiss, M. Mazzanti, Cell-permeable Ln(III) Chelate-functionalized InP quantum dots as multimodal imaging agents, ACS Nano 5 (2011) 8193–8201, https://doi.org/10.1021/NN202839W.

[5] F.G. Kinyanjui, S.T. Norberg, C.S. Knee, I. Ahmed, S. Hull, L. Buannic, I. Hung, Z. Gan, F. Blanc, C.P. Grey, S.G. Eriksson, Crystal structure and proton conductivity of $BaSn_{0.6}Sc_{0.4}O_{3-\delta}$: insights from neutron powder diffraction and solid-state NMR spectroscopy, J. Mater. Chem. A 4 (2016) 5088–5101, https://doi.org/10.1039/C5TA09744D.

[6] Y.H. Lai, C.Y. Su, H.W. Cheng, C.Y. Chu, L. Bin Jeng, C.S. Chiang, W.C. Shyu, S. Y. Chen, Stem cell–nanomedicine system as a theranostic bio-gadolinium agent for targeted neutron capture cancer therapy, Nat. Commun. 14 (2023) 1–17, https://doi.org/10.1038/s41467-023-35935-0.

[7] A. Magrasó, C.H. Hervoches, I. Ahmed, S. Hull, J. Nordström, A.W.B. Skilbred, R. Haugsrud, In situ high temperature powder neutron diffraction study of undoped and Ca-doped $La_{28-x}W_{4+x}O_{54+3x/2}$ (x = 0.85), J. Mater. Chem. A Mater. 1 (2013) 3774–3782, https://doi.org/10.1039/C3TA00497J.

[8] K. Kümmerer, E. Helmers, Hospital effluents as a source of gadolinium in the aquatic environment, Environ. Sci. Tech. 34 (2000) 573–577, https://doi.org/10.1021/ES990633H.

[9] Z. Fan, J.W. Shi, C. Gao, G. Gao, B. Wang, Y. Wang, C. He, C. Niu, Gd-modified MnOx for the selective catalytic reduction of NO by NH_3: The promoting effect of Gd on the catalytic performance and sulfur resistance, Chem. Eng. J. 348 (2018) 820–830, https://doi.org/10.1016/J.CEJ.2018.05.038.

[10] L. Henderson, O. Neumann, C. Kaffes, R. Zhang, V. Marangoni, M.K. Ravoori, V. Kundra, J. Bankson, P. Nordlander, N.J. Halas, Routes to potentially safer T1 magnetic resonance imaging contrast in a compact plasmonic nanoparticle with enhanced fluorescence, ACS Nano 12 (2018) 8214–8223, https://doi.org/10.1021/ACSNANO.8B03368.

[11] F. Chen, C. Yang, X. Liu, N. Zhang, P. Rong, S. Liang, R. Ma, Controllable fabrication of rare-earth-doped $Gd_2O_2SO_4$@SiO_2 double-shell hollow spheres for efficient upconversion luminescence and magnetic resonance imaging, ACS Sustain. Chem. Eng. 6 (2018) 10463–10471, https://doi.org/10.1021/ACSSUSCHEMENG.8B01828.

[12] Q. An, J. Liu, M. Yu, J. Wan, D. Li, C. Wang, C. Chen, J. Guo, Multifunctional magnetic Gd^{3+}-based coordination polymer nanoparticles: combination of magnetic resonance and multispectral optoacoustic detections for tumor-targeted imaging in vivo, Small 11 (2015) 5675–5686, https://doi.org/10.1002/SMLL.201501491.

[13] V.C. Pierre, M. Botta, S. Aime, K.N. Raymond, Fe(III)-templated Gd(III) self-assemblies - A new route toward macromolecular MRI contrast agents, J. Am. Chem. Soc. 128 (2006) 9272–9273, https://doi.org/10.1021/JA061323J.

[14] B. Henriques, L.S. Rocha, C.B. Lopes, P. Figueira, R.J.R. Monteiro, A.C. Duarte, M. A. Pardal, E. Pereira, Study on bioaccumulation and biosorption of mercury by living marine macroalgae: Prospecting for a new remediation biotechnology applied to saline waters, Chem. Eng. J. 281 (2015) 759–770, https://doi.org/10.1016/J.CEJ.2015.07.013.

[15] Y. Zhao, T. Niu, X. Dong, Y. Yang, W. Zhai, Robust graphene-drum bridged carbon aerogels for broadband acoustic and electromagnetic attenuation, J. Mater. Chem. A Mater. 11 (2023) 23452–23462, https://doi.org/10.1039/D3TA04895K.

[16] W. Chen, L. Wang, M. Zhuo, Y. Liu, Y. Wang, Y. Li, Facile and highly efficient removal of trace Gd(III) by adsorption of colloidal graphene oxide suspensions sealed in dialysis bag, J. Hazard. Mater. 279 (2014) 546–553, https://doi.org/10.1016/J.JHAZMAT.2014.06.075.

[17] Y. Li, R. Biswas, W.P. Kopcha, T. Dubroca, L. Abella, Y. Sun, R.A. Crichton, C. Rathnam, L. Yang, Y.W. Yeh, K. Kundu, A. Rodríguez-Fortea, J.M. Poblet, K. B. Lee, S. Hill, J. Zhang, Structurally defined water-soluble metallofullerene derivatives towards biomedical applications, Angew. Chem. Int. Ed. 62 (2023) e202211704, https://doi.org/10.1002/ANIE.202211704.

[18] C. Martino, R. Bonaventura, M. Byrne, M. Roccheri, V. Matranga, Effects of exposure to gadolinium on the development of geographically and phylogenetically distant sea urchins species, Mar. Environ. Res. 128 (2017) 98–106, https://doi.org/10.1016/J.MARENVRES.2016.06.001.

[19] V.V. Belova, Development of solvent extraction methods for recovering rare earth metals, Theor. Found. Chem. Eng. 51 (2017) 599–609, https://doi.org/10.1134/S004057951605002X.

[20] K. Li, Q. Gao, G. Yadavalli, X. Shen, H. Lei, B. Han, K. Xia, C. Zhou, Selective adsorption of Gd^{3+} on a magnetically retrievable imprinted chitosan/carbon nanotube composite with high capacity, ACS Appl. Mater. Interfaces 7 (2015) 21047–21055, https://doi.org/10.1021/ACSAMI.5B07560.

[21] M. Yang, Y. Zhou, D. Zhang, F. Zhou, H. Ning, M. He, R. Chi, W. Yin, Highly effective and selective recovery of Gd(III) from wastewater by defective MOFs-based ion-imprinted polymer: Performance and mechanism, Chem. Eng. J. 474 (2023) 145782, https://doi.org/10.1016/J.CEJ.2023.145782.

[22] X.H. Qi, K.Z. Du, M.L. Feng, Y.J. Gao, X.Y. Huang, M.G. Kanatzidis, Layered $A_2Sn_3S_7{\cdot}1.25H_2O$ (A = organic cation) as efficient ion-exchanger for rare earth element recovery, J. Am. Chem. Soc. 139 (2017) 4314–4317, https://doi.org/10.1021/JACS.7B00565.

[23] H. Vapnik, J. Elbert, X. Su, Redox-copolymers for the recovery of rare earth elements by electrochemically regenerated ion-exchange, J. Mater. Chem. A Mater. 9 (2021) 20068–20077, https://doi.org/10.1039/D1TA03334D.

[24] M.S. Nahar, J. Zhang, Recovery of trace metal isotopes in seawater samples using multifunctional neem (azadirachta indica) biosorbent: A comparison with monofunctional NOBIASChelatePA1 resin, ACS Sustain. Chem. Eng. 1 (2013) 488–495, https://doi.org/10.1021/SC3001433.

[25] R. Ganesh, K.G. Robinson, L. Chu, D. Kucsmas, G.D. Reed, Reductive precipitation of uranium by Desulfovibrio desulfuricans: evaluation of cocontaminant effects and selective removal, Water Res. 33 (1999) 3447–3458, https://doi.org/10.1016/S0043-1354(99)00024-X.

[26] A. Romero-Freire, V. González, J.E. Groenenberg, H. Qiu, M. Auffan, S. Cotelle, L. Giamberini, Cytotoxicity and genotoxicity of lanthanides for Vicia faba L. are mediated by their chemical speciation in different exposure media, Sci. Total Environ. 790 (2021) 148223. https://doi.org/10.1016/J.SCITOTENV.2021.148223.

[27] N. Lachaux, C. Catrouillet, R. Marsac, L. Poirier, S. Pain-Devin, E.M. Gross, L. Giamberini, Implications of speciation on rare earth element toxicity: A focus on organic matter influence in Daphnia magna standard test, Environ. Pollut. 307 (2022) 119554, https://doi.org/10.1016/J.ENVPOL.2022.119554.

[28] Y. Hu, E. Drouin, D. Larivière, F. Kleitz, F.G. Fontaine, Highly efficient and selective recovery of rare earth elements using mesoporous silica functionalized by preorganized chelating ligands, ACS Appl. Mater. Interfaces 9 (2017) 38584–38593, https://doi.org/10.1021/ACSAMI.7B12589.

[29] J.Y. Park, M.J. Baek, E.S. Choi, S. Woo, J.H. Kim, T.J. Kim, J.C. Jung, K.S. Chae, Y. Chang, G.H. Lee, Paramagnetic ultrasmall gadolinium oxide nanoparticles as advanced T 1 MRI contrast agent: Account for large longitudinal relaxivity, optimal particle diameter, and in Vivo T1 MR images, ACS Nano 3 (2009) 3663–3669, https://doi.org/10.1021/NN900761S.

[30] O.I.M. Ali, H.H. Osman, S.A. Sayed, M.E.H. Shalabi, The removal of some rare earth elements from their aqueous solutions on by-pass cement dust (BCD), J. Hazard. Mater. 195 (2011) 62–67, https://doi.org/10.1016/J.JHAZMAT.2011.08.014.

[31] J.H. Rademaker, R. Kleijn, Y. Yang, Recycling as a strategy against rare earth element criticality: A systemic evaluation of the potential yield of NdFeB magnet recycling, Environ. Sci. Tech. 47 (2013) 10129–10136, https://doi.org/10.1021/ES305007W.

[32] H. Cui, X. Zhang, J. Chen, X. Qian, Y. Zhong, C. Ma, H. Zhang, K. Liu, The construction of a microbial synthesis system for rare earth enrichment and material applications, Adv. Mater. 35 (2023) 2303457, https://doi.org/10.1002/ADMA.202303457.

[33] X. Zheng, E. Liu, F. Zhang, Y. Yan, J. Pan, Efficient adsorption and separation of dysprosium from NdFeB magnets in an acidic system by ion imprinted mesoporous silica sealed in a dialysis bag, Green Chem. 18 (2016) 5031–5040, https://doi.org/10.1039/C6GC01426G.

[34] E. Zhang, Y.C. Wu, H. Shao, V. Klimavicius, H. Zhang, P.L. Taberna, J. Grothe, G. Buntkowsky, F. Xu, P. Simon, S. Kaskel, Unraveling the capacitive charge storage mechanism of nitrogen-doped porous carbons by EQCM and ssNMR, J. Am. Chem. Soc. 144 (2022) 14217–14225, https://doi.org/10.1021/JACS.2C04841.

[35] S.M. Beladi-Mousavi, B. Khezri, S. Matějková, Z. Sofer, M. Pumera, Supercapacitors in motion: autonomous microswimmers for natural-resource recovery, Angew. Chem. Int. Ed. 58 (2019) 13340–13344, https://doi.org/10.1002/ANIE.201906642.

[36] M.Y. Chen, M.D. Klunk, V.M. Diep, M.J. Sailor, Electric-field-assisted protein transport, capture, and interferometric sensing in carbonized porous silicon films, Adv. Mater. 23 (2011) 4537–4542, https://doi.org/10.1002/ADMA.201102090.

[37] Y. Korenblit, A. Kajdos, W.C. West, M.C. Smart, E.J. Brandon, A. Kvit, J. Jagiello, G. Yushin, In situ studies of ion transport in microporous supercapacitor electrodes at ultralow temperatures, Adv. Funct. Mater. 22 (2012) 1655–1662, https://doi.org/10.1002/ADFM.201102573.

[38] M. Sun, A. Staykov, M. Yamauchi, Understanding the roles of hydroxide in CO_2 electroreduction on a Cu electrode for achieving variable selectivity, ACS Catal. 12 (2022) 14856–14863, https://doi.org/10.1021/ACSCATAL.2C03650.

[39] C.P. Byers, B.S. Hoener, W.S. Chang, S. Link, C.F. Landes, Single-particle plasmon voltammetry (spPV) for detecting anion adsorption, Nano Lett. 16 (2016) 2314–2321, https://doi.org/10.1021/ACS.NANOLETT.5B04990.

[40] C. Macías, G. Rasines, P. Lavela, M.C. Zafra, J.L. Tirado, C. Ania, Mn-containing N-doped monolithic carbon aerogels with enhanced macroporosity as electrodes for capacitive deionization, ACS Sustain. Chem. Eng. 4 (2016) 2487–2494, https://doi.org/10.1021/ACSSUSCHEMENG.5B01444.

[41] J. Lu, P. Kumar Mishra, T.N. Hunter, F. Yang, Z. Lu, D. Harbottle, Z., Xu, Functionalization of mesoporous carbons derived from pomelo peel as capacitive electrodes for preferential removal/recovery of copper and lead from contaminated water, Chem. Eng. J. 433 (2022) 134508, https://doi.org/10.1016/J.CEJ.2022.134508.

[42] J.E. Efome, D. Rana, T. Matsuura, C.Q. Lan, Metal–organic frameworks supported on nanofibers to remove heavy metals, J. Mater. Chem. A Mater. 6 (2018) 4550–4555, https://doi.org/10.1039/C7TA10428F.

[43] A. Macías-García, J.P. Carrasco-Amador, V. Encinas-Sánchez, M.A. Díaz-Díez, D. Torrejón-Martín, Preparation of activated carbon from kenaf by activation with H_3PO_4. Kinetic study of the adsorption/electroadsorption using a system of supports designed in 3D, for environmental applications, J. Environ. Chem. Eng. 7 (2019) 103196, https://doi.org/10.1016/J.JECE.2019.103196.

[44] J. Aburabie, S. Mohammed, A. Kumaran, R. Hashaikeh, From waste to wealth: chelating polymeric membranes for precious palladium recovery from wastewater, J. Mater. Chem. A Mater. 11 (2023) 22845–22858, https://doi.org/10.1039/D3TA04931K.

[45] C.C. Huang, J.C. He, Electrosorptive removal of copper ions from wastewater by using ordered mesoporous carbon electrodes, Chem. Eng. J. 221 (2013) 469–475, https://doi.org/10.1016/J.CEJ.2013.02.028.

[46] P. Li, Y. Gui, D.J. Blackwood, Development of a nanostructured α-MnO_2/carbon paper composite for removal of Ni^{2+}/Mn^{2+} ions by electrosorption, ACS Appl. Mater. Interfaces 10 (2018) 19615–19625, https://doi.org/10.1021/ACSAMI.8B02471.

[47] H. Wang, T. Yan, J. Shen, J. Zhang, L. Shi, D. Zhang, Efficient removal of metal ions by capacitive deionization with straw waste derived graphitic porous carbon nanosheets, Environ. Sci. Nano 7 (2020) 317–326, https://doi.org/10.1039/C9EN01233H.

[48] H.P. Chao, S.H. Chen, Adsorption characteristics of both cationic and oxyanionic metal ions on hexadecyltrimethylammonium bromide-modified NaY zeolite, Chem. Eng. J. 193–194 (2012) 283–289, https://doi.org/10.1016/J.CEJ.2012.04.059.

[49] A. Valverde, R. de Fernandez-de Luis, H. Salazar, B.F. Gonçalves, S. King, L. Almásy, M. Kriechbaum, J.M. Laza, J.L. Vilas-Vilela, P.M. Martins, S. Lanceros-Mendez, J.M. Porro, V.I. Petrenko, On the multiscale structure and morphology of PVDF-HFP@MOF membranes in the scope of water remediation applications, Adv. Mater. Interfaces 10 (2023) 2300424, https://doi.org/10.1002/ADMI.202300424.

[50] S. Elabbas, N. Ouazzani, L. Mandi, F. Berrekhis, M. Perdicakis, S. Pontvianne, M. N. Pons, F. Lapicque, J.P. Leclerc, Treatment of highly concentrated tannery wastewater using electrocoagulation: Influence of the quality of aluminium used for the electrode, J. Hazard. Mater. 319 (2016) 69–77, https://doi.org/10.1016/J.JHAZMAT.2015.12.067.

[51] M. Shang, B. Ma, X. Hu, L. Liu, J. Wang, X. Zhang, Biomimetic core-shell-structured nanofiber membranes for rapid and portable water purification, ACS Appl. Mater. Interfaces 14 (2022) 44849–44858, https://doi.org/10.1021/ACSAMI.2C12537.

[52] M. Mao, T. Yan, J. Shen, J. Zhang, D. Zhang, Selective capacitive removal of heavy metal ions from wastewater over lewis base sites of S-doped Fe-N-C cathodes via an electro-adsorption process, Environ. Sci. Tech. 55 (2021) 7665–7673, https://doi.org/10.1021/ACS.EST.1C01483.

[53] W. Zhan, X. Zhang, Y. Yuan, Q. Weng, S. Song, M. de J. Martínez-López, J.L. Arauz-Lara, F. Jia, Regulating chemisorption and electrosorption activity for efficient uptake of rare earth elements in low concentration on oxygen-doped molybdenum disulfide, ACS Nano 18 (2024) 7298–7310, https://doi.org/10.1021/ACSNANO.4C00691.

[54] W. Zhan, Y. Yuan, X. Zhang, Y. Liang, S. Song, M. de Jesús Martínez-López, J. L. Arauz-Lara, F. Jia, Efficient and selective Lead(II) removal within a wide concentration range through chemisorption and electrosorption coupling process via defective MoS_2 electrode, Sep. Purif. Technol. 329 (2024) 125183, https://doi.org/10.1016/J.SEPPUR.2023.125183.

[55] Q. Weng, S. Song, W. Zhan, X. Zhang, Z. Xiang, J. Gao, F. Jia, Novel recovery of a low-concentration gold thiosulfate complex through electroreduction via a walnut shell charcoal electrode, Green and Smart, Min. Eng. 1 (2024) 58–66, https://doi.org/10.1016/J.GSME.2024.03.004.

[56] M. Guo, Z. Xing, T. Zhao, Y. Qiu, B. Tao, Z. Li, W. Zhou, Hollow flower-like polyhedral α-Fe_2O_3/Defective MoS_2/Ag Z-scheme heterojunctions with enhanced photocatalytic-Fenton performance via surface plasmon resonance and photothermal effects, Appl. Catal. B 272 (2020) 118978, https://doi.org/10.1016/j.apcatb.2020.118978.

[57] S. Xu, D. Li, P. Wu, One-pot, facile, and versatile synthesis of monolayer MoS_2/WS_2 quantum dots as bioimaging probes and efficient electrocatalysts for hydrogen evolution reaction, Adv. Funct. Mater. 25 (2015) 1127–1136, https://doi.org/10.1002/adfm.201403863.

[58] Y. Chen, S. Huang, X. Ji, K. Adepalli, K. Yin, X. Ling, X. Wang, J. Xue, M. Dresselhaus, J. Kong, B. Yildiz, Tuning electronic structure of single layer MoS_2 through defect and interface engineering, ACS Nano 12 (2018) 2569–2579, https://doi.org/10.1021/ACSNANO.7B08418.

[59] W. Li, M.C. Tekell, Y. Huang, K. Bertelsmann, M. Lau, D. Fan, Synergistic high-rate solar steaming and mercury removal with MoS_2/C@polyurethane composite sponges, Adv. Energy Mater. 8 (2018) 1–11, https://doi.org/10.1002/aenm.201802108.

[60] X. Hong, J. Kim, S.F. Shi, Y. Zhang, C. Jin, Y. Sun, S. Tongay, J. Wu, Y. Zhang, F. Wang, Ultrafast charge transfer in atomically thin MoS_2/WS_2 heterostructures, Nat. Nanotechnol. 9 (2014) 682–686, https://doi.org/10.1038/nnano.2014.167.

[61] W. Zhan, F. Jia, Y. Yuan, C. Liu, K. Sun, B. Yang, Controllable incorporation of oxygen in MoS_2 for efficient adsorption of Hg^{2+} in aqueous solutions, J. Hazard. Mater. 384 (2020) 1–10, https://doi.org/10.1016/j.jhazmat.2019.121382.

[62] W. Zhan, Y. Yuan, C. Liu, P. Chen, Y. Liang, Y. Wang, J.L. Arauz-Lara, F. Jia, Preparation and application of 0D, 2D and 3D molybdenite: a review, Miner. Miner. Mater. 1 (2022) 5. https://doi.org/10.20517/mmm.2022.04.